CZECH TECHNICAL UNIVERSITY IN PRAGUE
Faculty of Nuclear Sciences and Physical Engineering

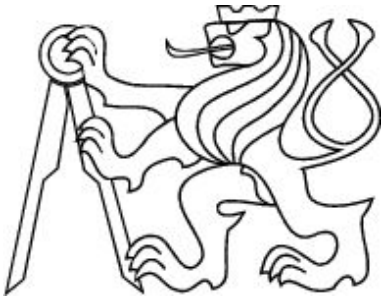

Research work

Study of the Energy Calibration Algorithm of Extreme Energy Cosmic Ray Showers

Prague, 2009 **Jakub Vícha**

Title: **Study of the Energy Calibration Algorithm of Extreme Energy Cosmic Ray Showers**

Author: Jakub Vícha

Field of study: Nuclear engineering

Specialization: Experimental nuclear physics

Type of work: Research work

Supervisor: RNDr. Petr Trávníček, PhD., Institute of Physics AS CR

Consultant: Ing. Michal Nyklíček, Institute of Physics AS CR

Abstract:

The energy calibration plays an important role in the study of the ultra high energy cosmic ray particles at the Pierre Auger Observatory. The uniqueness of the AUGER energy calibration lies in its independence on the hadronic interaction model due to the usage of experimental data only. The object of this work is to describe the energy calibration algorithm and to study application of the Constant Intensity Cut method on AUGER data to derive signal attenuation with respect to changing zenith angle. The attenuation curves from Monte Carlo simulated data for proton and iron of energies 10 EeV estimated for EPOS interaction model were compared with attenuation curves of corresponding energies obtained from experimental data.

Contents

Chapter 1

Introduction

The Pierre Auger Observatory (PAO) is the largest experiment for studying ultra-high energy cosmic rays ever built. The main objective of the project is to detect the cosmic ray particles with energy higher than $\sim 10^{18}$ eV. This is achieved throughout the measurement of secondary particle shower initiated in the earth atmosphere by primary particle.

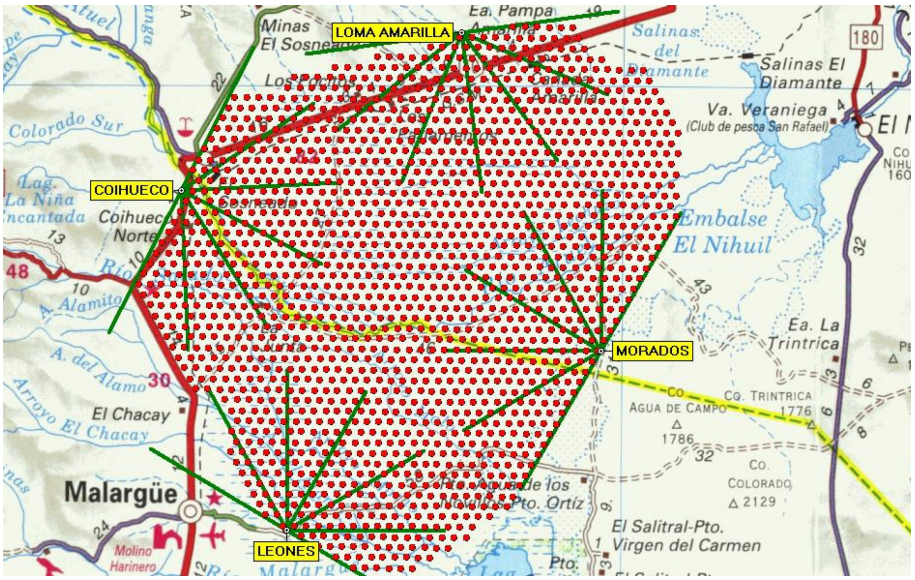

Figure 1.1: The view of the AUGER experiment. Red spots are representing tanks of the surface detector array, yellow labels are the names of 4 hills on which 4 fluorescence detectors are installed. The green lines demonstrate schematically the azimuthal field of view of the individual fluorescence telescopes. Picture is taken from [1].

The PAO is extended over an area of 3 000 km^2 in Argentina, province Mendoza, near the city Malargüe. The field of 1 600 tanks creates the giant Surface Detector (SD) which offers a large exposure[1]. Fluorescence Detector (FD) buildings are installed around this field at 4 hills (Fig. 1.1).

[1]The AUGER exposure was estimated to $\sim$ 17 600 km$^2\cdot$ s$\cdot$ y at 1. 7. 2009. This was approximately 10 times larger than the exposure of so far largest and recently completed experiment AGASA.

In the future, there is a plan to built a Northern site of the observatory for the full sky coverage. The southern site (AUGER) is operated in its designed size since autumn 2008, however the science data-taking was possible since the end of 2003 with smaller array.

1.1 Hybrid Detection

The most important characteristic of this experiment is the first continual usage of so called hybrid detection when the same shower is detected by surface and fluorescence detector simultaneously (Fig. 1.2). With this type of observation it is possible to achieve very high accuracy of the primary particle direction which allows to search for the anisotropy of the primary particle flux. Even more important aspect of the hybrid detection is the energy calibration of SD measurements by FD data as will be described in details in the next chapter.

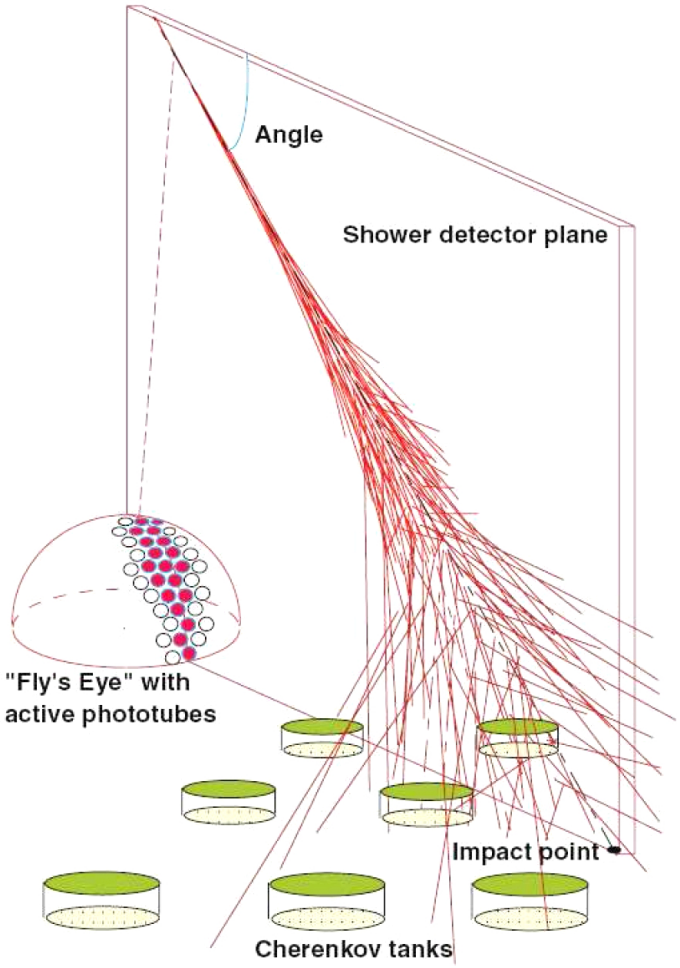

Figure 1.2: Schematic view of the hybrid detection. The shower is simultaneously detected in the fluorescence detector and in the surface detector array. Picture comes from [2].

Chapter 2

Energy Calibration at the Pierre Auger Observatory

The uniqueness of the SD energy calibration lies in its independence on the hadronic interaction models on which it was relied in all previous surface detector experiments of high energy cosmic rays. This is achieved through the precise FD energy measurement of hybrid events[1] and also by applying the Constant Intensity Cut (CIC) method used to get the Monte-Carlo independent SD energy estimator given by the function of zenith angle and measured signal size.

2.1 FD Measurement

One fluorescence detector building at AUGER consists of 6 fluorescence telescopes. Each of the telescopes gathers the light 30° in azimuthal and 28.6° in vertical direction. A spherical mirror of diameter 3.4 m focuses the light on the field of 440 photomultiplier tubes. Each photomultiplier pixel of hexagonal shape fills the view angle about $1.5° \times 1.5°$.

The highest fluorescence signal origins near the shower axis. Thus, after using the appropriate trigger, the shower axis is viewed as the path in the field of hexagonal pixels (Fig. 2.1). The energy is proportional to the signal of active pixels integrated over the path in the pixel field. Given the fluorescence yield the total signal can be directly converted to energy of the shower.

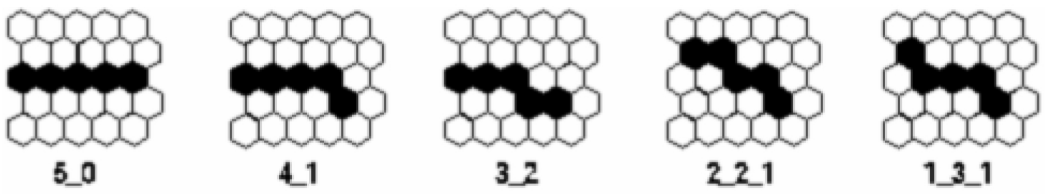

Figure 2.1: Fundamental 5-fold pixel patterns used in the FD trigger. Picture is taken from [3].

[1] More precisely the so called golden events as it will be explained further.

The FD telescopes are able to measure almost only during the moonless nights. They are very sensitive since they have to collect small fluorescence signals. Thus it is needed to protect them from the strong light background mainly from sunshine and moonlight. This is solved by closing the telescope shutters and lowering the voltages when the light background exceeds certain level. Therefore FD measures in duty cycle about 13 % of the time on the contrary to SD which are able to measure almost 100 % of the time.

2.2 SD Measurement

The surface detectors are cylindrical tanks of water used as the Cherenkov radiator medium. The Cherenkov light is produced when the charged shower particles traverse through the detector. The Cherenkov photons are reflected by the wall and ground of the detector and they are collected by 3 photomultipliers located in the roof of the detector.

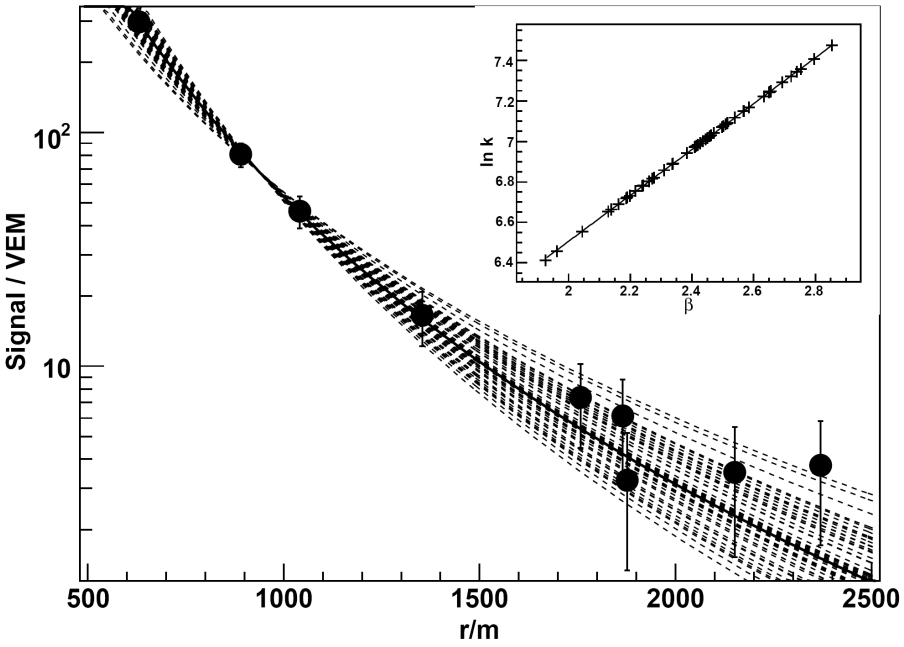

Figure 2.2: The same event 50 times reconstructed for different values of the slope parameter β of the LDF. The NKG type function of the LDF is used. The inset plot shows the relationship between the slope parameter β and the fitted size parameter k, allowing r_{opt} to be calculated analytically. The unit of the signal $S\,1000$ is VEM, which is the signal produced by muon of energy 250 MeV vertically penetrating the surface detector. For reference see [4].

The SD signal naturally decreases with the distance from the shower axis. This dependence is described with the Lateral Distribution Function (LDF). It can be parametrized by so called NKG[2]

[2]Named after Nishimura, Kamata and Greisen (1956).

function which has a form

$$S = k \cdot \left(\frac{r}{r_s}\right)^{-\beta} \left(1 + \frac{r}{r_s}\right)^{-\beta} \tag{2.1}$$

where S is the predicted signal, k the shower size parameter, β the slope parameter, r_s was set to 700 m and r is the distance from the shower axis.

Fig. 2.2 plots the signals of individual water Cherenkov detectors in case of given particular event as a function of their distance to shower core. The signals are fitted by equation (2.1) for different slope parameters β. The reasonable range of β parameter is obtained e.g. by the error assigned to it, if the β parameter is allowed to be free in the fit.

From the figure it follows that there is a distance around 1 000 m where the size of fluctuations given by different fits is minimal. Optimal distances of the similar sizes can be obtained for all events although they are somewhat depending on the particular event chosen. It was shown in [4] that the typical size of optimal distance depends on the spacing of the nearby detectors as it is illustrated in Fig. 2.3.

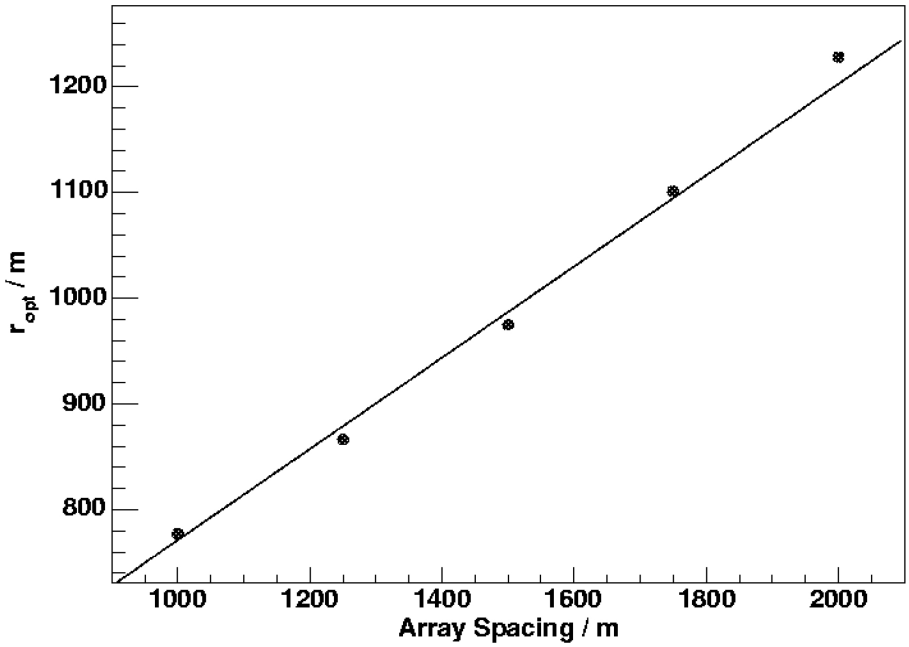

Figure 2.3: The dependence of the optimal ground parameter r_{opt} on the array spacing. The SD array with regular triangular grid is considered. Picture comes from [4].

For AUGER with SD arranged into the triangular grid with spacing 1 500 m [4] the optimal distances r_{opt} are close to 1 000 m for different events. Thus the LDF at 1 km (S 1000) is a good choice for further energy conversion with minimum fluctuations (Fig. 2.2) emerging from the uncertainty of the fitted LDF.

The signal $S1000$ is also dependent on the zenith angle of the shower axis. This dependence is called the attenuation curve and is gained applying the Constant Intensity Cut method as will be explained in the next chapter.

For the conversion of $S1000$ to the energy of the shower some reference value is therefore needed. The reference value ($S38$) was chosen as the $S1000$ signal of the same shower if it would arrive with zenith angle 38° which is the median zenith angle of all events.

2.3 Energetic Calibration of the SD

The sample of hybrid events is much smaller compared to the sample of SD only events. Moreover it is necessary to use another selection criteria to ensure the best precision together with sample of events large enough to be able to make some reliable conclusions.

2.3.1 Golden Events

For the SD energy calibration only a subset of hybrid events is used. The so called golden events have to fulfill these basic features:

- zenith angle $\leq 60°$,
- energy $\geq 3 \cdot 10^{18}$ eV,
- accomplishing the T5 trigger condition.

The other essential conditions can be found in [5].

Zenith angle The zenith angle less than 60° together with the energy threshold assures that the aperture calculations for hybrid events are only of the geometrical character. They are then not dependent on the energy and the zenith angle.

Energy The energy cut is also set to ensure that all of the hybrid events will be detected. Whereas at $2.5 \cdot 10^{18}$ eV the overall trigger efficiency is 90 %, at $3 \cdot 10^{18}$ eV the efficiency is greater than 99 %.

Trigger T5 With this "physical" trigger it is guaranteed that the ground (shower core) is intersected by the shower axis within the SD field. The T5 trigger requires that at least 5 nearest tanks are active among the tank with the highest signal of the detected shower (Fig. 2.4).

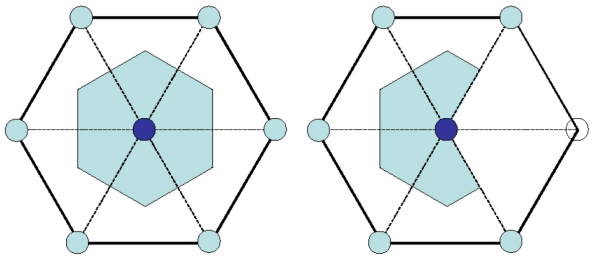

Figure 2.4: T5 trigger condition. On the left there is a situation when the tank with the highest signal is surrounded with all active 6 nearest tanks. On the right there is a case with 5 of 6 surrounding active tanks. Picture is taken from [6].

2.3.2 SD Calibration Curve

As it has been previously mentioned, the signal $S38$ is proportional to the energy. The general calibration equation has the form

$$S38 = a \cdot E_{FD}^{b}\,, \tag{2.2}$$

where a and b are constants determined from the fit at Fig. 2.5 and E_{FD} is the energy measured with FD.

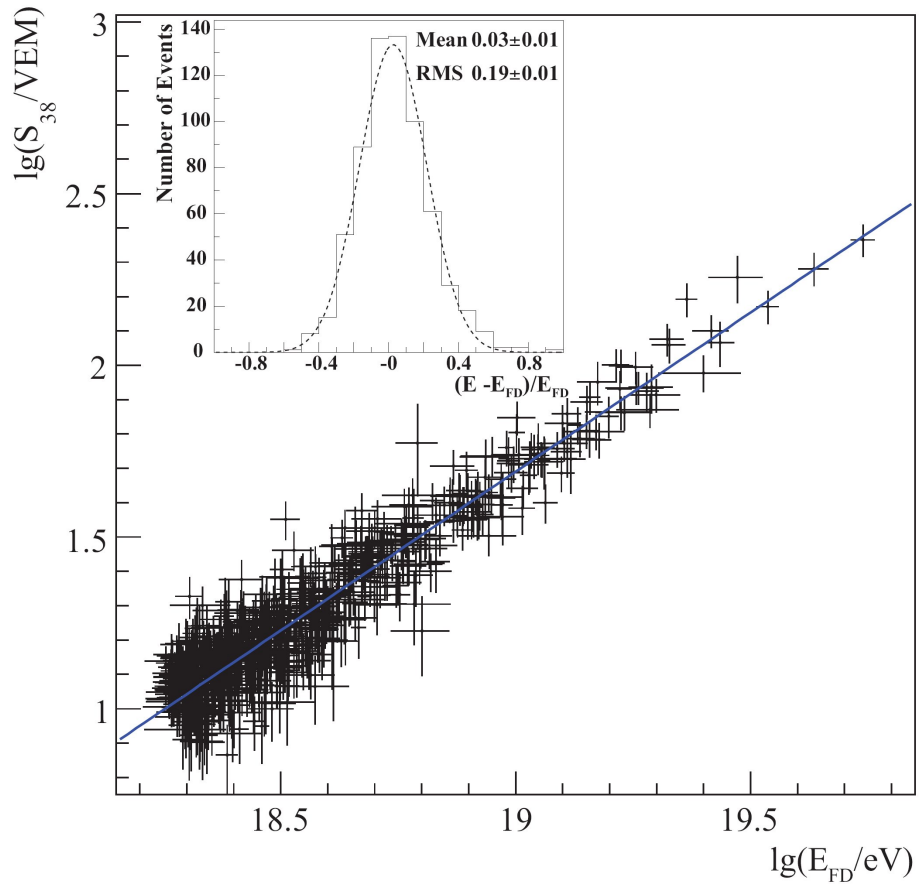

Figure 2.5: Plot of the SD energy calibration. The dependence of the logarithm $S38$ on the logarithm of the fluorescence energy E_{FD} is shown for 661 golden hybrid events. The fractional differences between the two energy estimators are inset (E denotes the energy from the SD). Picture comes from [7].

a [10^{-1} EeV]	b [-]
1.49	1.08

Table 2.1: Fit parameters in equation (2.2) set from Fig. 2.5. For reference see [7].

Chapter 3

Attenuation Curve

This chapter provides the original results of the research work obtained by the author. The attenuation curve is the dependence of the $S\,1000$ on the zenith angle Θ for a given primary particle energy or on a function of the zenith angle[1]. This dependence can be acquired from the simulation data or from the real data using the Constant Intensity Cut method.

3.1 Constant Intensity Cut Method

The Constant Intensity Cut method assumes the isotropic flux of primary cosmic ray particles above a given energies. The originally used technique plots the event flux for bins of $cos^2(\Theta)$ for various event selection. This selection is determined by different minimum value of the parameter $S\,1000$ (Fig. 3.1). The intersections of the curves corresponding to different minimal $S\,1000$ with a horizontal line, given by the chosen flux, give the attenuation curve. The resulting attenuation curve is dependent on the chosen cut and also on the precision with which the intersections are actually found.

Another technique lies in sorting the $S\,1000$ from the biggest to the lowest value for every bin of $cos^2(\Theta)$. Choosing the N^{th} value (cut) of the $S\,1000$ for every bin the attenuation curve is set. This method was used for producing the attenuation curves in this work.

3.1.1 Technical Information of Produced Attenuation Curves

All the further plots are normalized to 1 at the zenith angle 38° which corresponds to the value of $cos^2(\Theta) = 0.62096$. The attenuation curves from experimental data are produced for bins of $cos^2(\Theta)$ of size 0.05. For fitting the χ^2 method was used. The vertical error bars of points were produced as the differences of the $S\,1000$ at the $(N + \sqrt{N})^{th}$ or $(N - \sqrt{N})^{th}$ position from the $S\,1000$ at the N^{th} position in ordered bins. Half bin size was set as the symmetric horizontal error bar.

[1] Mostly $cos^2(\Theta)$ is used in this work since a bin of $cos^2(\Theta)$ corresponds to the element of space angle.

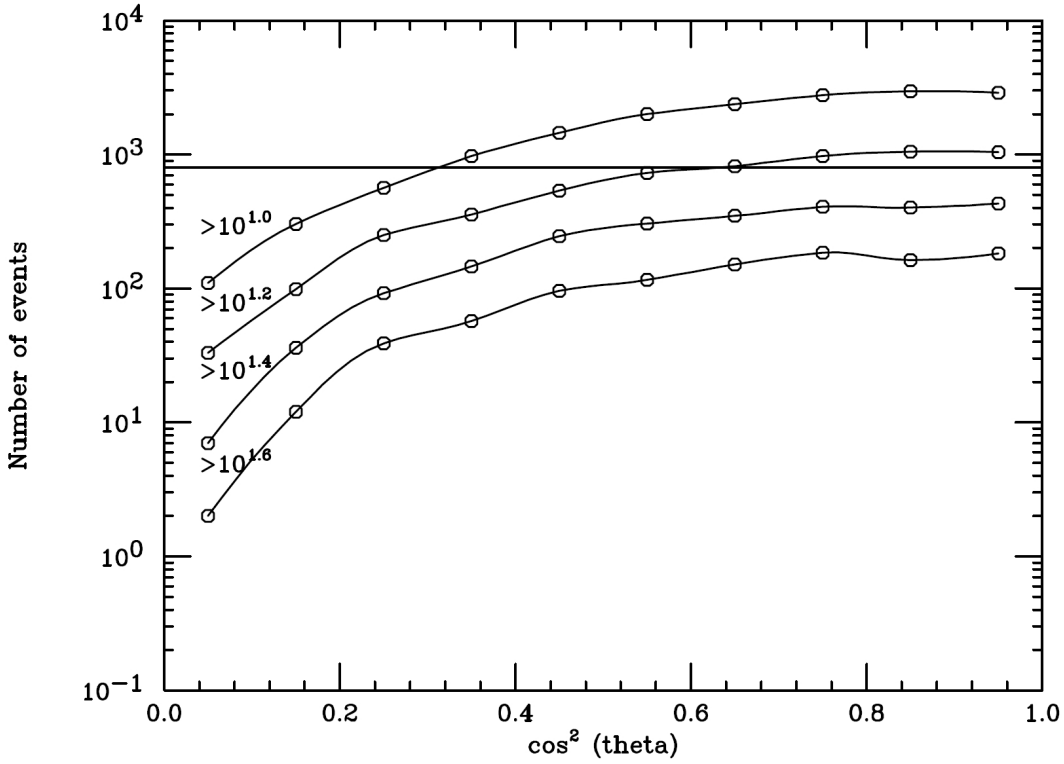

Figure 3.1: Plot of integral number of events vs. $cos^2(\Theta)$ for the indicated minimum value of $S\,1000$. The horizontal line represents the constant flux. Picture comes from [8].

3.2 Experimental Data

The data collected between 1. 1. 2004 and 9. 3. 2008 at the Pierre Auger Observatory were used to determine the attenuation curves. "SD only" events satisfying the condition for zenith angle $< 60°$ were selected from the Tribune data format.

The objective of this work was to try own method based on event sorting and to study the dependence of the resulting curve on chosen cut (Fig. 3.2). Obtained attenuation curves are compared with previous studies [8], [5] in Fig. 3.3.

The $S\,38$ value was inferred from the polynomial fit of the second order as the fit value at the zenith angle 38°. For the estimation of energy equivalent to chosen cut the conversion from the equation (2.1) with parameters from Tab. 2.1 was used. As could be seen from Fig. 3.2 the attenuation curves occur to have similar shape. Especially it can be said that the uncertainty in the shape of the attenuation curve is less then 10 % given the arbitrary chosen cut.

Moreover for many plots with different cuts in range from 100 to $\sim$ 1500 no notable deviation in shape of the attenuation curves was noticed. It was shown in [9] that the flux is anisotropic for cosmic rays of energy higher than 56 EeV with probability almost 100 %. Thus weaker cut than 100 corresponds to too high energy and would be therefore unsuitable for the used CIC method due to basic demand - isotropic flux of cosmic rays.

The obtained results are in a very good agreement with attenuation curves from [8] and [5]. This confirms the validity of used CIC method application. Little deviations are probably mainly caused by different sets of events and by different sizes of bin $cos^2(\Theta)$.

	a	b	c
N = 155	- 1.13334	2.3379	- 0.0147363
N = 230	- 1.23692	2.432	- 0.0332273
N = 700	- 1.1435	2.30359	0.010486
N = 1150	- 1.02892	2.17403	0.0467558

Table 3.1: Values of used fit parameters satisfying the equation: $y = a \cdot x^2 + b \cdot x + c$, where $y = S1000/S38$ and $x = cos^2(\Theta)$ valid in range from 0.25 to 1. N denotes the value of the cut.

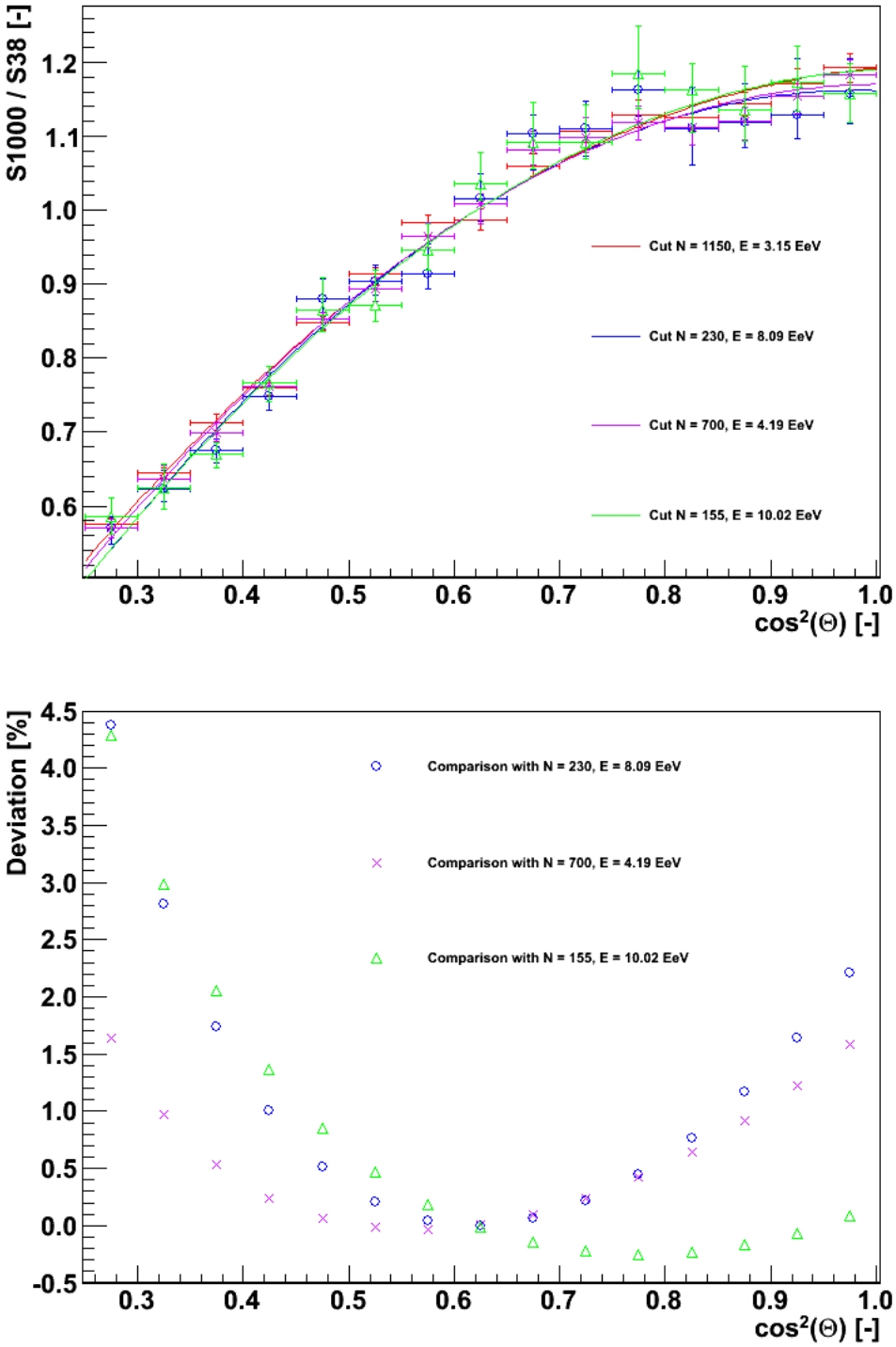

Figure 3.2: Top: Attenuation curves determined for 4 different cuts N corresponding to different energies E. Fit parameters can be found in Tab. 3.1. Bottom: Relative deviations of attenuation curve points. Under these relative deviations the value of $\frac{CIC_{1150}-CIC_N}{CIC_{1150}} \cdot 100\%$ is considered for every value of bin $cos^2(\Theta)$, where under CIC the normalized value of $S\,1000$ is meant and the subindex denotes the cut.

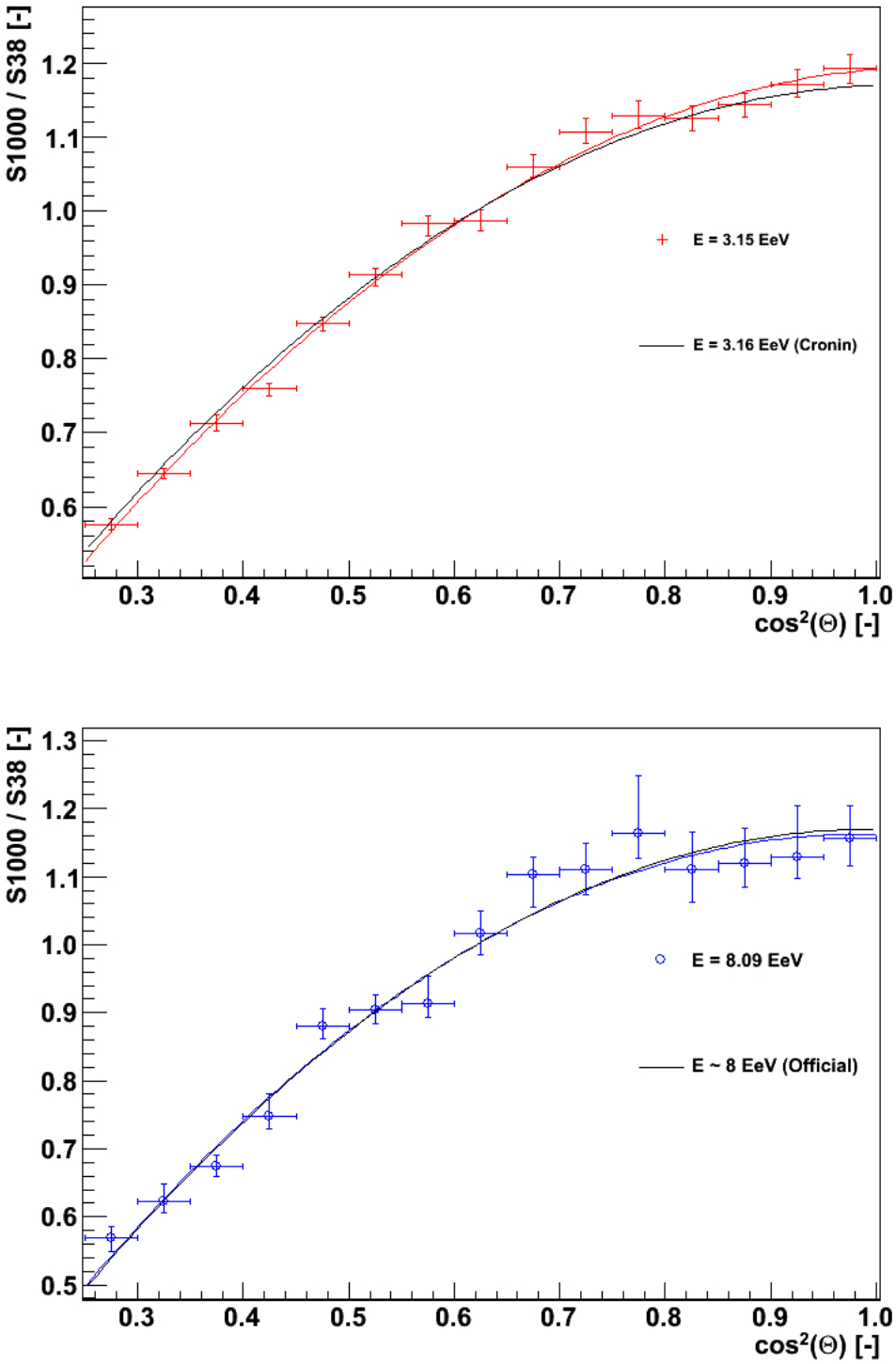

Figure 3.3: The attenuation curves from the experimental data in comparison with the attenuation curves gained from experimental data by Cronin [8] (top) and [5] (bottom). The latter is denoted as the "Official attenuation curve" for showers of energy 8 EeV. The corresponding energies E are shown. Fit parameters can be found in Tab. 3.1.

3.3 Attenuation Curve from Simulated Data

The data obtained from simulations for showers initiated by proton (Fig. 3.4) and iron (Fig. 3.5) were used. The primary particles of showers were set to have the energy 10 EeV and the zenith angle of produced showers was set in steps in $cos^2(\Theta)$ from 0.25 to 1. This data were simulated by the Czech Group of AUGER in the simulation program CORSIKA. The hadronic interaction model EPOS was used for high energy collisions and the model FLUKA was used for the low energetic processes in the shower development. In the end the inputs from CORSIKA were used in the program Offline for simulating the resulting signal in the surface detector.

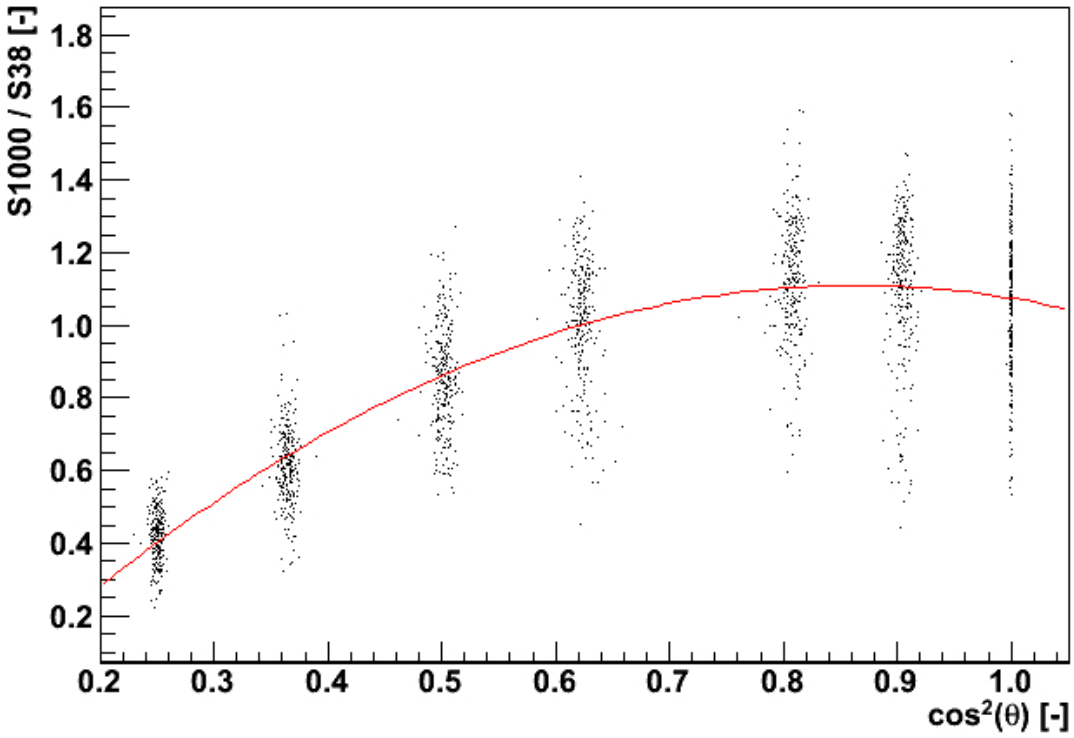

Figure 3.4: Simulated values of the $S\,1000$ in dependence on $cos^2(\Theta)$ for showers initiated by proton of energy 10 EeV. The fitted attenuation curve from 1 716 simulated events is shown. Fit parameters can be found in Tab. 3.2.

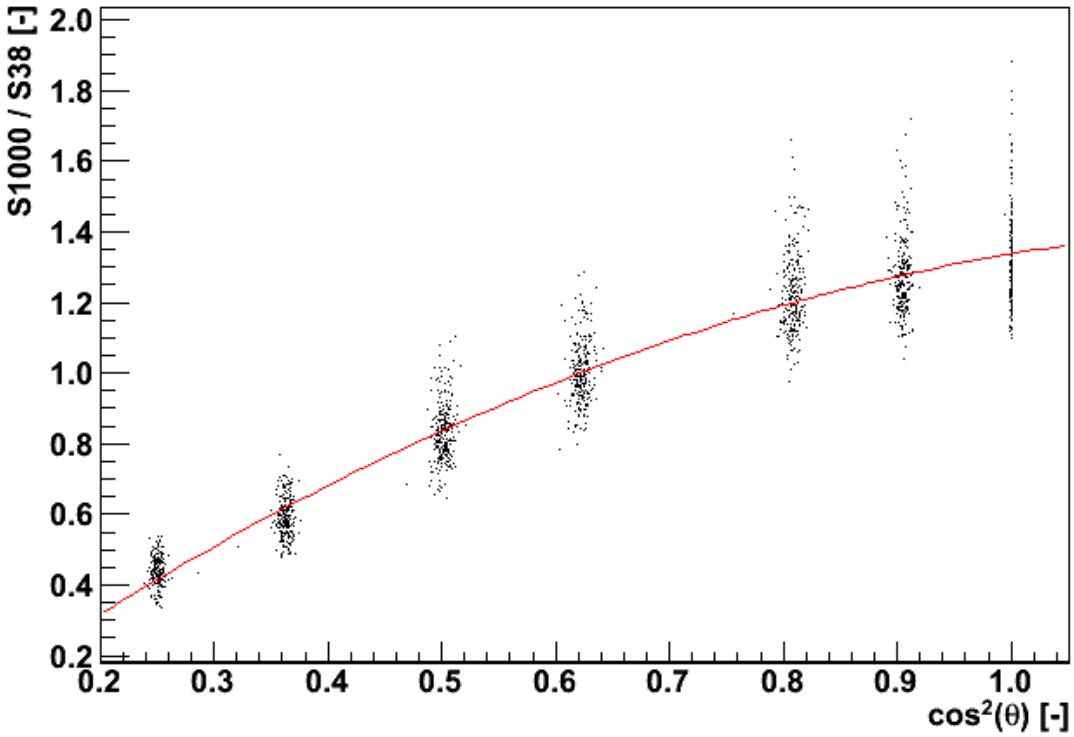

Figure 3.5: Simulated values of the $S\,1000$ in dependence on $cos^2(\Theta)$ for showers initiated by iron of energy 10 EeV. The fitted attenuation curve from 1 684 simulated events is shown. Fit parameters can be found in Tab. 3.2.

	a	b	c
p	- 1.88683	3.25644	- 0.294572
Fe	- 0.912625	2.36984	- 0.119676

Table 3.2: Values of used fit parameters satisfying the equation: $y = a \cdot x^2 + b \cdot x + c$, where $y = S\,1000/S\,38$ and $x = cos^2(\Theta)$ valid in range from 0.25 to 1. p denotes simulated data for showers initiated by proton and Fe so as by iron.

3.4 Comparison of Simulated and Experimental Data

For the curve shape determination the normalized curves are suitable due to the elimination of the signal size energy dependence. Shapes of the attenuation curves (Fig. 3.6) for proton and iron are in agreement with real data only in a region about 38° which is assured from the definition of normalization. For inclined events both curves from simulated data fall faster then the curve from real data. Relative deviations can be found in Fig. 3.7. For vertical showers little "flattening" is remarkable for experimental data. It seems that this trend is rather followed by simulated data for proton whereas the attenuation curve for iron increases steeply over the attenuation curve for experimental data. Regardless, neither of both curves from simulated data does not describe the shape of attenuation curve from experimental data adequately.

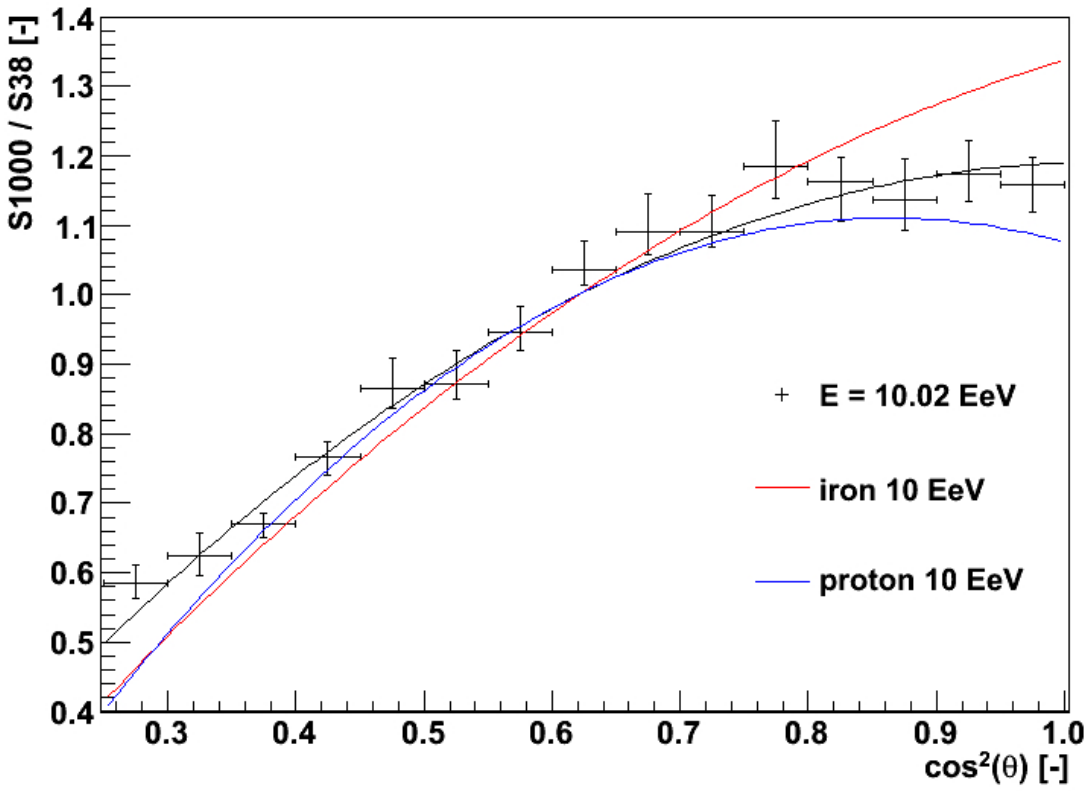

Figure 3.6: Comparison of the attenuation curves from simulated showers initiated by proton and iron of energies 10 EeV with the attenuation curve set from experimental data using the cut corresponding to energy ~ 10 EeV. Curves are normalized to satisfy the condition $S38 = 1$. Fit parameters can be found in Tab. 3.1 and Tab. 3.2.

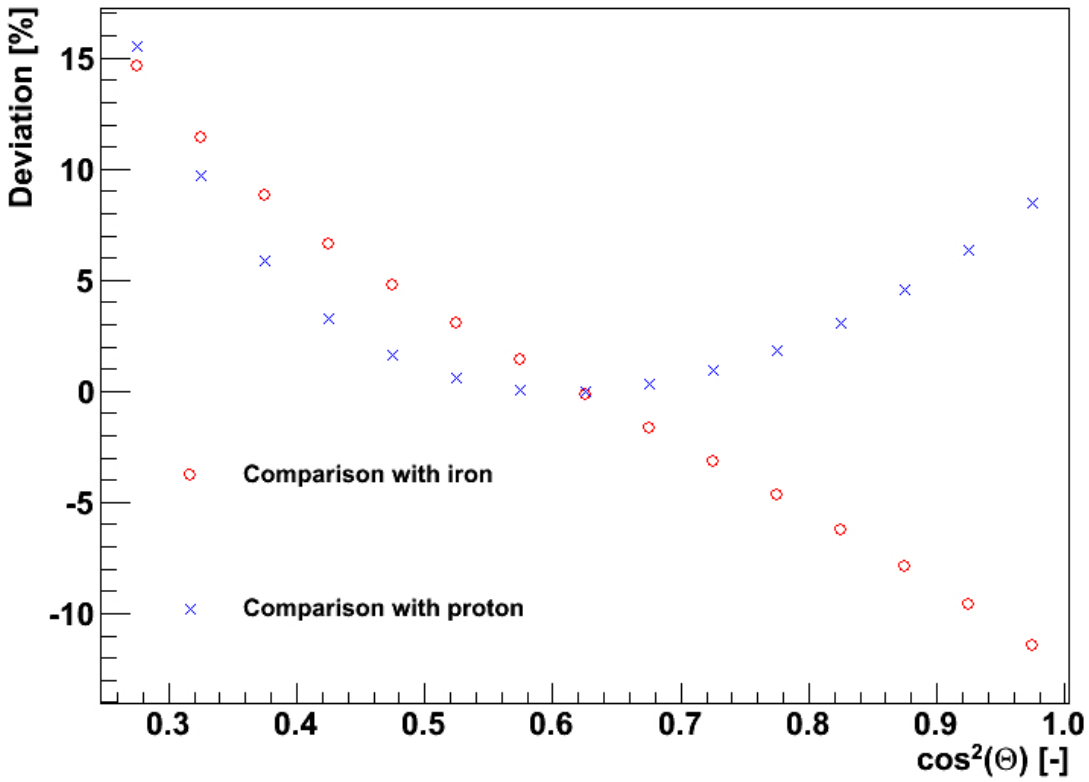

Figure 3.7: Relative deviations of attenuation curve points of simulated data from real data. Curves from Fig. 3.6 were used. Under these relative deviations the value of $\frac{CIC_{real}-CIC_{simulated}}{CIC_{real}} \cdot 100\%$ is considered for every value of bin $cos^2(\Theta)$, where under CIC the normalized value of $S\,1000$ is meant and the subindex distinguish the type of data. Simulated data for showers initiated by proton and iron were used.

Chapter 4

Conclusions

The energy calibration of the Surface Detector at the Pierre Auger Observatory was described. The usage of hybrid detected events permits to calibrate the SD energy without any assumption from Monte Carlo simulations.

The application of the Constant Intensity Cut method based on event sorting was successfully applied to AUGER data. The applicability of this variation of the CIC method was shown for 4 different cuts. The dependence of the attenuation curve on the chosen cut was found to be less then 10 %.

For energy 10 EeV the hadronic model EPOS does not fully describe the shape of the attenuation curve from real data. The attenuation curves from MC data with EPOS differs at zenith angles $\sim 60°$ up to 20 % from the curve obtained from real data using CIC method.

Bibliography

[1] The Auger Collaboration, *The Pierre Auger Observatory Design Report*, Fermilab, (1997).

[2] Haungs A., Rebel H. a Roth M., *Energy spectrum and mass composition of high-energy cosmic rays*, Rept. Prog. Phys. 66, pp. 1145-1206, (2003).

[3] The Auger Collaboration, *Technical Design Report*, draft version, pp. 1-491, (2004).

[4] Newton D., Knapp J., Watson A. A., *The Optimum Distance at which to Determine the Size of a Giant Air Shower*, arXiv:astro-ph/0608118v1, (2006).

[5] Denia M. M., *Energy calibration of the Pierre Auger Observatory. Measurement of the spectrum of the Ultra-High Energy Cosmic Rays*, doctoral thesis, (2008).

[6] Allard D. et al., Proceedings of the *29th International Cosmic Ray Conference Pune*, fra-parizot-E-abs1-he14-poster, (2005).

[7] Pierre Auger Collaboration, *Observation of the suppression of the flux of cosmic rays above* $4 \cdot 10^{19}$ *eV*, Phys. Rev. Lett. 101, (2008).

[8] Cronin J. W., Yamamoto T., *Simulation-independent determination of the cosmic ray spectrum for energies above* $2 \cdot 10^{18}$ *eV*, draft version, (2006).

[9] The Pierre Auger Collaboration, *Correlation of the Highest-Energy Cosmic Rays with Nearby Extragalactic Objects*, Science 318: 938-943, (2007).